The changes in variables of interest (for example, IC) should be assessed for stability properties, such as resistance[15]. Our results show that this method is a rigorous and effective way to analyse food-web structure and provide the initial steps in understanding the relationship between compartments and stability[1–5]. □

Methods

Interactions were weighted by interaction frequency, by carbon flow or by interaction strength. Interaction frequency was estimated as acts of predation per hectare per day[26]. Carbon flow from prey i' to predator i, $W_{ii'}$, was estimated as $\mathrm{g\,C\,m^{-2}\,yr^{-1}}$ (refs 27, 28). Interaction strength was the geometric mean of the interaction strengths between predator i and prey i' (ref. 30). The interaction strength of predator i on prey i' was measured as $-(W_{ii'}/B_i)$, where B_i is the biomass of predator i ($\mathrm{g\,C\,m^{-2}}$), and the interaction strength of prey i' on predator i was measured as $R_i(W_{ii'}/B_{i'})$, where $B_{i'}$ is the biomass of prey i' ($\mathrm{g\,C\,m^{-2}}$) and R_i is the production to consumption ratio of predator i (ref. 30). With weights, the definition of IC becomes the proportion of possible interactions, each with maximum weight, that are realized (with no cannibalistic interactions).

We used the software KliqueFinder[12] to identify compartments. Because KliqueFinder operates on an integer scale from 1 to 99,999 we modified the interactions for weighted versions of the food webs to fit the scale. The modifications had little or no effect on the results. To test whether the concentration of interactions within identified compartments was greater than what was likely to have occurred by chance alone, for each web we conducted Monte Carlo simulations. First, we randomly reassigned interactions, constraining the row marginal (sum of each row in a matrix) to be equal to the row marginal of the original food web, where rows represented predators and columns represented prey. We then applied KliqueFinder and recorded the odds ratio. We then repeated this process 1,000 times to obtain a sampling distribution against which we could compare the empirical odds ratio. Our constraints ensured that the simulated food webs had the same number of predators, the same number (and weight) of interactions associated with a predator, and the same total number (and weight) of realized interactions as the original food web. Basal taxa (taxa with no prey) did vary in simulations for some food web versions, which did change the overall IC from the original for some food webs but we found that there was little or no effect on the P values and no effect on statistical inference.

Although the range of calibrating simulations[12,14] (the third feature of the methodology) did not allow a direct assessment of the performance of the algorithm for our data (because of large n and weighted interactions), the algorithm typically performs well when there is evidence of compartments in non-weighted data[12]. Cannibalism and taxa that interacted with only one other taxon were dropped from the analysis when optimizing the odds ratio because these interactions do not add information to the relative assignments of taxa to compartments. Dropped taxa were added back to the food web for the calculations in Table 2.

Coordinates for the diagram in Fig. 1 were generated by employing multidimensional scaling within and between subgroups[13], and SAS proc gplot was used to generate the figure. Because of the large magnitude of the difference between the smallest and largest interaction strength weightings (~10,000-fold), the lines were weighted by the rank of the associated interaction strength, where the smallest interaction strength was given a rank of 1 and the largest a rank of 137 (the maximal number of realized interactions). The units are based on the inverse of the between-compartment density (0.0097).

In our scenarios for exploring compartments and stability, we made one simple assumption: the predators of the taxon involved in the disturbance compensated for the loss in their interactions by increasing their interaction strength with their remaining prey items. For the first hypothetical scenario, all interactions with taxon 36 were removed and the predators on 36 had their interaction strengths associated with 36 redistributed proportionally to their other prey interactions. For the second hypothetical scenario, all interactions associated with taxon 6 were removed except for those with taxa 5 and 8. The interactions of the predators on 6 were modified in the same manner as in the first scenario.

Received 12 June; accepted 10 October 2003; doi:10.1038/nature02115.

1. Pimm, S. L. The structure of food webs. *Theor. Popul. Biol.* **16,** 144–158 (1979).
2. May, R. M. *Stability and Complexity in Model Ecosystems* (Princeton Univ. Press, 1973).
3. Simon, H. A. in *General Systems: Yearbook of the Society for General Systems* (eds von Bertalanffy, L. & Rapaport, A.) Vol. 10 63–76 (Society for General Systems, Ann Arbor, Michigan, 1965).
4. McNaughton, S. J. Stability and diversity of ecological communities. *Nature* **274,** 251–252 (1978).
5. Simmel, G. *The Sociology of Georg Simmel* (transl. and ed. Wolff, K. H.) (Free Press, Glencoe, Illinois, 1950).
6. Pimm, S. L. & Lawton, J. H. Are food webs divided into compartments? *J. Anim. Ecol.* **49,** 879–898 (1980).
7. Yodiz, P. The compartmentation of real and assembled ecosystems. *Am. Nat.* **120,** 551–570 (1982).
8. Raffaelli, D. & Hall, S. J. Compartments and predation in an estuarine food web. *J. Anim. Ecol.* **61,** 551–560 (1992).
9. Dicks, L. V., Corbet, S. A. & Pywell, R. F. Compartmentalization in plant–insect flower visitor webs. *J. Anim. Ecol.* **71,** 32–43 (2002).
10. Moore, J. C. & Hunt, H. W. Resource compartmentation and the stability of real ecosystems. *Nature* **333,** 261–263 (1988).
11. Girvan, M. & Newman, M. E. J. Community structure in social and biological networks. *Proc. Natl Acad. Sci. USA* **99,** 8271–8276 (2002).
12. Frank, K. Identifying cohesive subgroups. *Soc. Networks* **17,** 27–56 (1995).
13. Frank, K. Mapping interactions within and between cohesive subgroups. *Soc. Networks* **18,** 93–119 (1996).
14. Frank, K. & Yasumoto, J. Y. Linking action to social structure within a system: social capital within and between groups. *Am. J. Sociol.* **104,** 642–686 (1998).
15. Grimm, V. A down-to-earth assessment of stability concepts in ecology: dreams, demands, and the real problems. *Senckenbergiana maritima* **27,** 215–226 (1996).
16. McCann, K. S. The diversity–stability debate. *Nature* **405,** 228–233 (2000).
17. Dunne, J. A., Williams, R. J. & Martinez, N. D. Network structure and biodiversity loss in food webs: robustness increases with connectance. *Ecol. Lett.* **5,** 558–567 (2002).
18. Johnson, J. C., Borgatti, S. P., Luczkovich, J. J. & Everett, M. G. Network role analysis in the study of food webs: an application of regular role coloration. *J. Soc. Structure* **2;** published online at ⟨http://zeeb.library.cmu.edu:7850/JoSS/johnson/RoleAnalysis.html⟩ (2001).
19. McMahon, S. M., Miller, K. H. & Drake, J. Networking tips for social scientists and ecologists. *Science* **293,** 1604–1605 (2001).
20. Simmel, G. *Conflict and the Web of Group Affiliations* transl. Wolff, K. (Free Press, Glencoe, Illinois, 1955).
21. Blau, P. M. *Inequality and Heterogeneity* (Macmillan, New York, 1977).
22. Martinez, N. D. Artifacts or attributes? Effects of resolution on the Little Rock Lake food web. *Ecol. Monogr.* **61,** 367–392 (1991).
23. Raffaelli, D. From Elton to mathematics and back again. *Science* **296,** 1035–1037 (2002).
24. Huxham, M., Beaney, S. & Raffaelli, D. Do parasites reduce the chances of triangulation in a real food web? *Oikos* **76,** 284–300 (1996).
25. Williams, R. J. & Martinez, N. D Simple rules yield complex food webs. *Nature* **404,** 180–183 (2000).
26. Goldwasser, L. & Roughgarden, J. Construction and analysis of a large Caribbean food web. *Ecology* **74,** 1216–1233 (1993).
27. Ulanowicz, R. E. & Baird, D. Nutrient controls on ecosystem dynamics: the Chesapeake mesohaline community. *J. Mar. Syst.* **19,** 159–172 (1999).
28. Abarca-Arenas, L. G. & Ulanowicz, R. E. The effects of taxonomic aggregation on network analysis. *Ecol. Modell.* **149,** 285–296 (2002).
29. Polis, G. A. Complex trophic interactions in deserts: an empirical critique of food-web theory. *Am. Nat.* **138,** 123–155 (1991).
30. Neutel, A. M., Heesterneek, J. A. P. & de Ruiter, P. C. Stability in real food webs: weak links in long loops. *Science* **296,** 1120–1123 (2002).

Supplementary Information accompanies the paper on **www.nature.com/nature**.

Acknowledgements We thank M. Huxham and D. Raffaelli for providing data on the Ythan Estuary food web; N. Martinez and J. Dunne for providing data on the Little Rock Lake food webs; L. Abarca-Arenas for providing data on the 45-taxa Chesapeake Bay food web; C. Darnell for enhancing the diagram; and C. Goddard and J. Liu for comments and suggestions. This work was supported by the Great Lakes Fishery Commission (A.E.K., D.M.M.), the National Institute of Child Health and Human Development (K.A.F.) and the National Science Foundation (K.A.F.). Opinions reflect those of the authors and do not necessarily reflect those of the granting agency.

Competing interests statement The authors declare that they have no competing financial interests.

Correspondence and requests for materials should be addressed to A.E.K. (krausean@msu.edu).

Activation of the TRPC1 cation channel by metabotropic glutamate receptor mGluR1

Sang Jeong Kim[1,2], Yu Shin Kim[1], Joseph P. Yuan[1], Ronald S. Petralia[3], Paul F. Worley[1] & David J. Linden[1]

[1]*Department of Neuroscience, Johns Hopkins University School of Medicine, 725 N. Wolfe Street, Baltimore, Maryland 21205, USA*
[2]*Department of Physiology, Kangwon National University School of Medicine, Chunchon, 200-71, Korea*
[3]*NIDCD/NIH, Building 50, Room 4142 50 South Drive, MSC 8027, Bethesda, Maryland 20892, USA*

Group I metabotropic glutamate receptors (consisting of mGluR1 and mGluR5) are G-protein-coupled neurotransmitter receptors[1] that are found in the perisynaptic region of the post-synaptic membrane[2]. These receptors are not activated by single synaptic volleys but rather require bursts of activity[3–5]. They are implicated in many forms of neural plasticity including hippocampal long-term potentiation and depression[6–8], cerebellar long-term depression[8–11], associative learning[7,11], and cocaine addiction[12]. When activated, group I mGluRs engage two G-protein-dependent signalling mechanisms: stimulation of phospholipase C and activation of an unidentified, mixed-cation

excitatory postsynaptic conductance (EPSC), displaying slow activation, in the plasma membrane[4,5,13–15]. Here we report that the mGluR1-evoked slow EPSC is mediated by the TRPC1 cation channel. TRPC1 is expressed in perisynaptic regions of the cerebellar parallel fibre–Purkinje cell synapse and is physically associated with mGluR1. Manipulations that interfere with TRPC1 block the mGluR1-evoked slow EPSC in Purkinje cells; however, fast transmission mediated by AMPA-type glutamate receptors remains unaffected. Furthermore, co-expression of mGluR1 and TRPC1 in a heterologous system reconstituted a mGluR1-evoked conductance that closely resembles the slow EPSC in Purkinje cells.

In cerebellar Purkinje cells, mGluR1 is linked via a $G\alpha_q$ protein complex to the activation of phospholipase Cβ (PLC-β), which cleaves the membrane phospholipid phosphatidylinositol-4,5-bisphosphate to yield 1,2-diacylglycerol and inositol-1,4,5-trisphosphate ($InsP_3$). Activation of mGluR1 by burst stimulation of parallel fibres results in both Ca^{2+} mobilization through a PLC-β–$InsP_3$ cascade[16–18] and activation of a slow EPSC[3] carried by a mixed-cation conductance[4,5,13–15]. The identity of the ion channel underlying the mGluR1-evoked slow EPSC has not been determined in Purkinje cells or in any other cell type. There are, however, a number of observations that constrain the identity of the ion channel underlying the slow EPSC. It is a mixed-cation conductance that reverses at about +20 mV (refs 5, 14, 15) and requires external Ca^{2+} (refs 5, 19). It is not blocked by antagonists of Na^+/Ca^{2+} exchangers, purinergic receptors, hyperpolarization-activated cation channels or voltage-gated Ca^{2+} channels[5,13,15].

There are several reasons to believe that the Ca^{2+} mobilization and slow EPSC signals evoked by mGluR1 activation are dependent on $G\alpha_q$ but subsequently involve divergent pathways. First, drugs that interfere with PLC-β, $InsP_3$ receptors or internal Ca^{2+} stores completely block Ca^{2+} mobilization but have variable effects on the slow EPSC conductance, ranging from no blockade to weak blockade[4,5,13–15]. Second, photolysis of caged $InsP_3$ or Ca^{2+} does not mimic the slow EPSC[15]. Third, drugs[4,13] and induced mutations[20] that inhibit $G\alpha_q$ block both Ca^{2+} mobilization and the slow EPSC. Fourth, weak burst stimulation of parallel fibres can evoke Ca^{2+} mobilization in the absence of the slow EPSC, whereas stronger burst stimulation recruits both signals (ref. 16 and S.J.K., P.F.W. and D.J.L., unpublished observations).

Group I mGluRs are organized at glutamatergic synapses through interactions with scaffolding molecules, most notably the Homer family of proteins, which form multimers capable of regulating

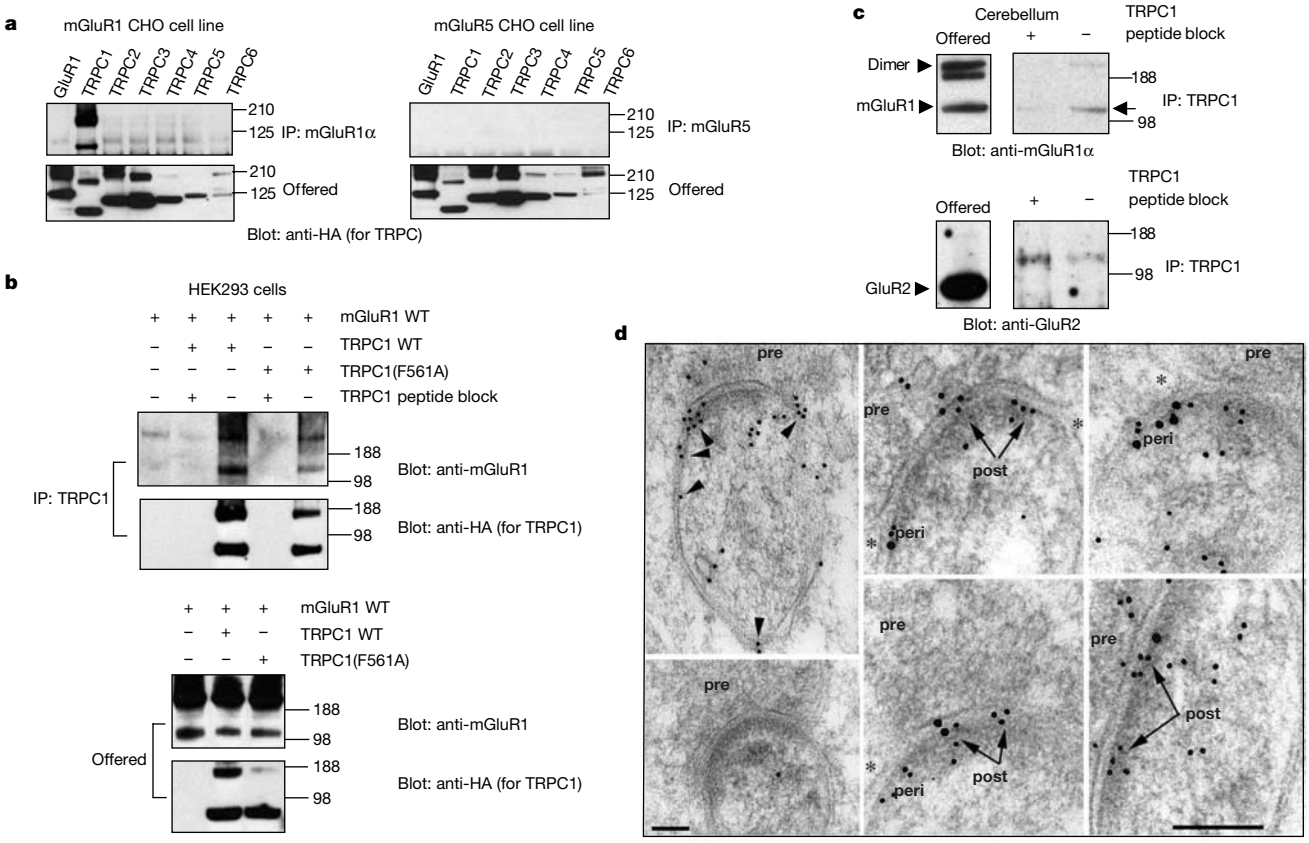

Figure 1 mGluR1α and TRPC1 physically associate in CHO cells, HEK293 cells and in brain, and they co-localize on Purkinje cell spines. **a**, mGluR1α- and mGluR5-expressing CHO cell lines were transfected with haemagglutinin (HA)-tagged TRPC1−6. HA–TRPC1, but not GluR1 or other TRPCs, co-immunoprecipitate with mGluR1α. None of the TRPCs co-immunoprecipitate with mGluR5. Markers are in kDa. **b**, HEK293 cells were transfected with mGluR1α and/or HA–TRPC1 (WT or F561A). TRPC1 and TRPC1(F561A) co-immunoprecipitate mGluR1α. Anti-TRPC1 antibody does not immunoprecipitate mGluR1α in the absence of TRPC1. **c**, TRPC1 co-immunoprecipitates mGluR1α (arrow) but not GluR2 (overexposed and displaying a nonspecific band greater than the size of GluR2) from cerebellum. Preabsorption of TRPC1 antibody with peptide antigen reduced mGluR1α by 90%. **d**, The left column shows immunogold labelling for TRPC1 associated with spine synapses in the molecular layer of the cerebellum. Arrowheads indicate labelling with 10 nm F(ab′)2-gold associated with the perisynaptic as well as extrasynaptic and outer synaptic membrane areas of the postsynaptic spine. Sections were labelled with antibody without (left panel, top row) and with (left panel, bottom row) preabsorption with peptide. Pre, presynaptic terminal. Scale bar: 100 nm. The middle and right columns show co-localization of immunogold labelling for TRPC1 (5 nm) and mGluR1α (10 nm) associated with spine synapses in the molecular layer of the cerebellum. Arrows indicate postsynaptic labelling (post). Peri refers to perisynaptic/extrasynaptic labelling of the spine membrane near glia processes (asterisks) adjacent to the synaptic cleft. Some labelling for TRPC1 is also seen in the presynaptic terminals (pre). Scale bar: 100 nm.

coupling of group I mGluRs to a number of targets including $InsP_3$ receptors, ryanodine receptor and voltage-gated calcium channels[21]. In recent studies we found that Homer also binds and regulates the gating of members of the TRPC family of nonspecific cation channels[22]. TRPC channels are activated in response to G-protein-coupled receptor activation and/or depletion of intracellular Ca^{2+} stores, and are believed to participate in replenishment and regulation of intracellular Ca^{2+} pools in a process termed capacitive calcium entry[23]. TRPC1 is expressed in cerebellar Purkinje cells[24]. Accordingly, we examined the hypothesis that a TRPC ion channel underlies the mGluR1-evoked slow EPSC.

CHO cell lines that stably express mGluR1α or mGluR5 were transfected with TRPC1, TRPC2, TRPC3, TRPC4, TRPC5 or TRPC6. mGluR1α antibody co-immunoprecipitated TRPC1 but not other TRPCs, whereas mGluR5 antibody did not co-immunoprecipitate any of the TRPC channels (Fig. 1a). mGluR1α and TRPC1 also co-immunoprecipitated using a TRPC1 antibody (Fig. 1b). These data indicate a specific physical interaction between TRPC1 and mGluR1α. A TRPC1 mutant lacking channel activity (described below) showed similar association with mGluR1α. To determine whether mGluR1α and TRPC1 associate *in vivo*, we assayed for co-immunoprecipitation of mGluR1α from detergent lysates of cerebellum using TRPC1 antibodies (Fig. 1c). TRPC1 antibody co-immunoprecipitated mGluR1α and this was blocked by TRPC1 peptide. TRPC1 antibody did not co-immunoprecipitate the AMPA (α-amino-3-hydroxy-5-methyl-4-isoxazole propionic acid) receptor subunit GluR2. To assess the ultrastructural localization of TRPC1 we performed post-embedding immuno-electron microscopy on adult rat cerebellum (Fig. 1d). Gold particles preferentially localized to dendritic spines of Purkinje neurons where they co-localized with mGluR1α along the spine membrane. Co-localization was evident in the perisynaptic region as well as at the postsynaptic membrane. These biochemical and anatomical data make TRPC1 an attractive candidate for the ion channel underlying the mGluR1-evoked slow EPSC. Indeed, this suggestion has been made previously based on the similarity of a current recorded in a heterologous cell expressing TRPC1 and either TRPC4 or TRPC5 (ref. 24) to that recorded in hippocampal[25] or midbrain dopaminergic[26] neurons stimulated with a group I mGluR agonist.

We next examined the mGluR1-evoked EPSC in Purkinje neurons of acute cerebellar slices using whole-cell patch clamp. Stimulation of parallel fibres with a brief burst gives rise to a fast component predominantly mediated by AMPA receptors and a slow component mediated by mGluR1. In some cases the falling phase of the fast component overlaps the rising phase of the slow component, making it difficult to measure them separately. To facilitate our analysis of the delayed EPSC, we applied the AMPA/kainate receptor antagonist CNQX (6-cyano-7-nitroquinoxaline-2,3-dione) at a concentration that produces an approximately 90% reduction in the amplitude of the fast EPSC (10 μM). This allowed for clearly

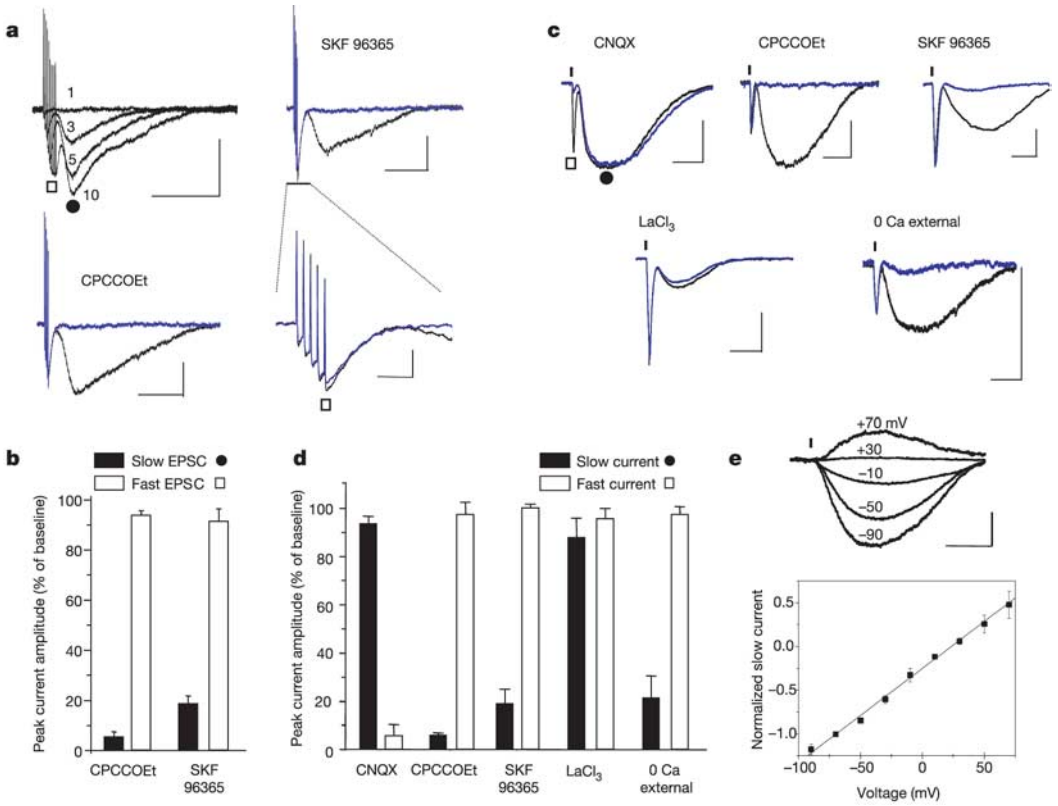

Figure 2 Characterization of the mGluR1-evoked slow EPSC in Purkinje cells. **a**, Representative single traces show fast and slow components of the parallel-fibre-evoked EPSC which were produced by burst stimulation at 100 Hz in the presence of CNQX (10 μM) and GABAzine (5 μM). A burst consisting of five pulses was adopted as the standard stimulus. The black traces represent the pretreatment (baseline) condition whereas the blue traces represent the post-treatment condition at an asymptotic time point (typically 5–12 min after introduction of the treatment). Numbers in the top left panel indicate number of pulses. Scale bars: 100 pA, 0.5 s, except for the time-expanded traces in the lower right panel (50 ms). **b**, Population data for the manipulations shown in **a** are expressed as the percentage of baseline peak current amplitude and are presented as mean ± s.e.m. **c**, Fast and slow inward currents were evoked by micropressure pulses (10 p.s.i., 50 ms duration) of external solution containing DHPG (100 μM) and glutamate (40–100 μM) delivered through a patch pipette. Representative current traces are shown before (black) and after (blue) various bath-applied treatments. Scale bars: 200 pA, 0.5 s. **d**, Population data for the manipulations shown in **c** are expressed as the percentage of baseline peak current amplitude. **e**, Upper panel shows the DHPG-evoked slow currents at different potentials in the presence of TTX (1 μM), NBQX (20 μM), $CdCl_2$ (200 μM) and $BaCl_2$ (5 mM, by replacing $CaCl_2$). Scale bars: 200 pA, 0.5 s. Lower panel shows current–voltage relations for a population of five Purkinje cells. Current has been normalized to the value at −70 mV. Linear regression line is shown in the plot.

resolvable fast and slow EPSC components (Fig. 2a, b). The amplitude of the stimulation current was adjusted to evoke a 300–500 pA fast EPSC in the absence of CNQX. A burst frequency of 100 Hz was used to maximize the slow EPSC[6] and the holding potential was set to −70 mV. As previously reported[3,4], single stimuli of parallel fibres did not evoke a measurable slow EPSC, and the amplitude of the slow EPSC depended on the number of pulses in the train. Bath application of an mGluR1 antagonist, CPCCOEt (100 μM), completely abolished the slow EPSC evoked by a train of five stimuli (4.9 ± 1.9% of baseline, mean ± s.e.m., $n = 7$ cells, within-cell comparisons). A nonselective antagonist of receptor-operated cation channels, SKF 96365 (30 μM), also strongly blocked the mGluR-evoked slow EPSC (18.6 ± 3.0% of baseline, $n = 13$ cells). The inhibitory effects of both CPCCOEt and SKF 96365 on the slow EPSC were selective, having no effect on the peak amplitude of the fast EPSC (93.8 ± 1.8%, $n = 7$ cells; 90.2 ± 6.4%, $n = 10$ cells, respectively).

To evaluate specifically postsynaptic responses, and to avoid possible effects of manipulations on presynaptic release, mGluRs were activated by micropressure pulses of 3,5-dihydroxyphenylglycine (DHPG, 100 μM; 10 pounds per square inch (p.s.i.), 50 ms) delivered through a patch pipette. Glutamate (40–100 μM) was included in this solution to produce a small, fast inward current, serving as a control measure for nonspecific effects (Fig. 2c, d). Similar to results with the EPSC evoked by burst stimulation of parallel fibres, CPCCOEt (100 μM) and SKF 96365 (30 μM) blocked the mGluR-evoked slow current (5.9 ± 1.0%, $n = 6$ cells; 18.9 ± 6.1%, $n = 8$ cells, respectively) but left the fast current unaffected. $LaCl_3$, which blocks voltage-gated calcium channels and augments some, but not all, TRPC channels in heterologous expression systems[24], did not significantly attenuate either the fast or slow component of the inward current (95.7 ± 4.3%; 88.0 ± 8.0%, $n = 5$ cells, respectively). Removal of external calcium attenuated the slow current (21.5 ± 9.0%, $n = 5$ cells) but did not affect the fast current (97.5 ± 6.4%, $n = 5$ cells). The current–voltage relation of the slow current in Purkinje cells was roughly linear and reversed at about +23 mV, consistent with a previous report[15]. These properties of the mGluR1-evoked slow current in Purkinje cells are consistent with a conductance mediated by TRPC1, but they do not uniquely implicate TRPC1, nor do they exclude some other candidate ion channels.

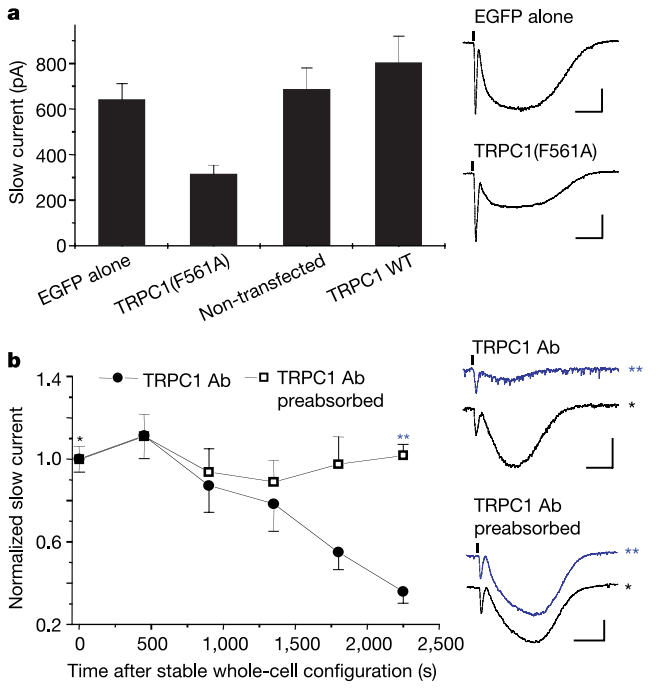

Figure 3 Manipulations that interfere with TRPC1 function block the mGluR1-evoked slow current in Purkinje cells. **a**, Population data in four different conditions are expressed as the peak amplitude of mGluR1-evoked slow current in Purkinje cells in organotypic slice cultures. The amplitude of slow current from cells transfected with a dominant-negative pore mutant of TRPC1 (TRPC1(F561A)) was attenuated in comparison to that of cells transfected with EFGP alone, non-transfected cells and cells transfected with wild-type TRPC1. Representative single-current traces are shown to the right. Scale bars: 200 pA, 0.5 s. **b**, Time course of the amplitude of the slow current that was activated by micropressure pulses of DHPG together with glutamate. The current amplitude was normalized to the value recorded immediately after achieving a stable whole-cell configuration. Representative current traces are shown to the right. Scale bars: 200 pA, 0.5 s. Ab, antibody. Representative current traces are shown before (black) and after (blue) various treatments.

To examine the role of TRPC1 in the mGluR1-evoked current, Purkinje neurons in slice culture were transfected with an expression construct of the channel mutant TRPC1(F561A) (Fig. 1b) along with enhanced green fluorescent protein (EGFP; Fig. 3a). In control cells transfected with EGFP alone and stimulated with micropressure pulses of DHPG plus glutamate, the peak amplitude of the slow current was 640 ± 72 pA ($n = 10$ cells). In cells expressing TRPC1(F561A), the amplitude of mGluR-evoked slow current was reduced to 49% of that measured in an EGFP-alone control (313 ± 39 pA, $n = 33$ cells, $P < 0.001$). The amplitude of slow currents in non-transfected Purkinje cells (686 ± 95 pA, $n = 9$ cells) and in cells transfected with wild-type TRPC1 (802 ± 116 pA, $n = 11$ cells) was significantly larger than that of cells transfected with TRPC1(F561A) ($P < 0.001$ for both), and was not significantly different from cells transfected with EGFP alone ($P > 0.10$ for both).

To provide an independent test for the role of TRPC1, we included TRPC1 antibody (30 μg ml^{-1}) in the pipette solution and performed whole-cell recordings from Purkinje cells in organotypic culture (Fig. 3b). In a separate group of cells we applied the antibody rendered nonfunctional by preabsorption with TRPC1 peptide. In TRPC1-antibody-treated cells the amplitude of the slow current started to decrease about 15 min after achieving stable whole-cell recording. At 37.5 min, the difference between the normalized slow current with antibody preabsorbed with TRPC1 peptide (nonfunctional; 1.02 ± 0.06, $n = 6$ cells) and that with TRPC1 antibody (0.36 ± 0.06, $n = 6$ cells) was statistically significant ($P < 0.01$). This time course probably reflects the diffusion of TRPC1 antibody from the pipette to the dendritic site of mGluR1 activation.

As a further test of the hypothesis that TRPC1 underlies the mGluR1-evoked slow EPSC, we attempted to reconstitute this conductance in a heterologous system. A line of CHO cells constitutively expressing mGluR1 was co-transfected with EGFP and TRPC1. EGFP-positive cells were subjected to whole-cell patch-clamp recording. A command potential of −70 mV was imposed, and mGluR1 was activated with a micropressure pulse of DHPG (10 p.s.i., 100 ms). This evoked a slowly activating inward current with a peak current density of 19.3 ± 3.9 pA pF^{-1} (mean ± s.e.m., $n = 8$ cells; Fig. 4a, b). TRPC5 is reported to form heteromultimers with TRPC1 (ref. 27), and CHO cells transfected with both TRPC1 and TRPC5 displayed an even larger DHPG-evoked current (50.7 ± 7.8 pA pF^{-1}, $n = 7$ cells). In contrast, when a separate population of CHO cells was transfected with TRPC3—a related channel that does not form a complex with mGluR1—no significant inward current was evoked (0.5 ± 0.5 pA pF^{-1} and 0.2 ± 0.3 pA pF^{-1}, respectively, $n = 6$ cells per group). Transfection with TRPC1(F561A) similarly yielded no significant current (0.4 ± 0.3 pA pF^{-1}, $n = 7$). When TRPC1 was transfected together with TRPC1(F561A) in a ratio of 2:1, the amplitude of the evoked slow current was reduced to about 25% of that seen with TRPC1 alone (4.8 ± 2.5 pA pF^{-1}, $n = 6$). This is similar to the effect of

TRPC1(F561A) transfection in Purkinje cells (Fig. 3). The current–voltage relation for TRPC1/TRPC5-transfected CHO cells (not shown) revealed that the DHPG-evoked current was roughly linear and reversed at about +23 mV, similar to the mGluR1 EPSC in Purkinje cells (Fig. 2 and ref. 22). Both CPCCOEt (100 μM) and SKF 96365 (50 μM) completely abolished the DHPG-evoked current (5 ± 4% of baseline, $n = 7$ cells; 3 ± 3% of baseline, $n = 8$ cells, respectively). The DHPG-evoked current was not significantly altered by $LaCl_3$ (100 μM; 91 ± 9% of baseline, $n = 7$ cells). Removal of external calcium, previously shown to attenuate the slow EPSC in Purkinje cells[7,28] (see Fig. 2c, d), produced a near-complete blockade of the DHPG-evoked current (13 ± 4% of baseline, $n = 7$ cells). Notably, internal application of a TRPC1-inactivating antibody (30 μg ml^{-1}), but not a control solution consisting of antibody preabsorbed with TRPC1 peptide, produced a strong attenuation of DHPG-evoked current (26 ± 4% of baseline, $n = 6$; 109 ± 8% of baseline, $n = 7$, respectively).

Biochemical studies demonstrate a selective interaction of mGluR1 with TRPC1 (Fig. 1a). To assess whether mGluR1 may be selectively capable of activating TRPC1, we performed simultaneous voltage-clamp and ratiometric calcium imaging of CHO cells expressing TRPC1 with other G-protein receptors, including mGluR5 or M1 muscarinic receptor. In cells expressing mGluR5 and TRPC1, DHPG application resulted in a robust calcium transient (568 ± 155 nM, peak free calcium, $n = 10$ cells; thereby confirming that mGluR5 was functionally expressed) but no significant activation of membrane current (0.9 ± 0.8 pA pF^{-1}). When this experiment was repeated with cells expressing mGluR1, strong calcium responses (783 ± 145 nM, $n = 10$) and a robust inward current (25.3 ± 4.6 pA pF^{-1}) were observed, similar to that previously seen using a CHO cell line engineered to stably express mGluR1 (Supplementary Fig. 1). When this experiment was repeated with cells expressing M1 muscarinic receptor in place of mGluR, and stimulation with the muscarinic agonist pilocarpine in place of DHPG, the results were similar to that seen with mGluR5 (that is, a strong calcium signal was observed (696 ± 88 nM, $n = 10$) but no significant membrane current accompanied this calcium transient (0.6 ± 0.5 pA pF^{-1})). These findings show that not all G_q/PLC-coupled receptors can activate the TRPC1-mediated slow conductance, and they suggest that the specific physical association of mGluR1 and TRPC1 is important for signal coupling.

Our observations indicate that TRPC1 is required for the mGluR1-induced inward current in Purkinje neurons. Because TRPC1 is known to co-assemble with TRPC4 and TRPC5, it is possible that the native channel is a heteromultimer[24,27]. Furthermore, although it is likely that the slow EPSC evoked by group I mGluR activation in Purkinje cells is similar to that in other neurons, there may be some important differences as well. For example, the slow EPSC recorded in hippocampal pyramidal neurons seems to require activation of both mGluR1 and

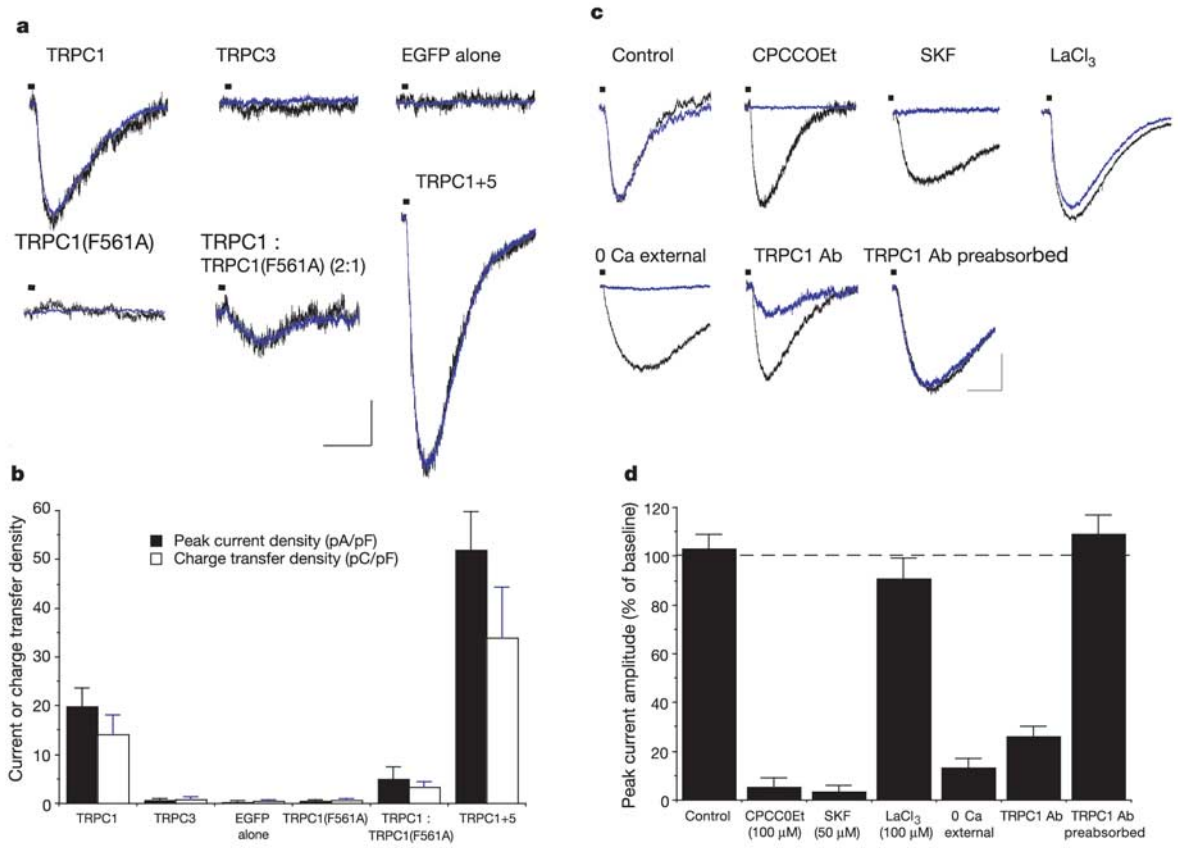

Figure 4 The inward current evoked by DHPG in mGluR1/TRPC1-expressing CHO cells closely resembles the mGluR1-evoked slow EPSC in Purkinje cells. **a**, Representative current traces in a line of CHO cells that constitutively expressed mGluR1 together with the indicated ion channels. Micropressure pulses of DHPG were delivered as indicated by the horizontal bars (100 ms, 10 p.s.i.). Black traces are single sweeps and blue traces are the average of six consecutive sweeps. Scale bars: 50 pA, 1 s. **b**, Population data for the manipulations shown in **a** normalized to cell membrane capacitance (as an index of plasma membrane surface area) and presented as mean ± s.e.m. **c**, Representative current traces for experiments using within-cell comparisons for CHO cells expressing TRPC1 together with mGluR1. In this panel all traces are the average of six consecutive sweeps. The black trace represents the pre-treatment condition whereas the blue trace represents the post-treatment condition at an asymptotic time point (typically 5–12 min after introduction of the treatment). Scale bars: 50 pA, 1 s. **d**, Population data for the manipulations shown in **c** are expressed as the percentage of baseline peak current amplitude.

mGluR5 to produce a maximal effect[25] whereas Purkinje cells only express mGluR1.

What is the function of the mGluR-evoked slow EPSC? One possibility is that the Ca^{2+} influx associated with this current serves to replenish internal stores depleted by activation of the PLC–$InsP_3$ signalling cascade. In other cell types this is accomplished by direct coupling between calcium stores and TRPC channels[23]. In Purkinje cells the relationship between activation of the PLC–$InsP_3$ cascade and the TRPC1 cascade is less clear, as manipulations that interfere with PLC-β, $InsP_3$ receptors or internal Ca^{2+} stores have weak and variable effects on the slow EPSC conductance[4,5,13–15]. It is also possible that the Ca^{2+} and/or Na^{+} influx mediated by the slow EPSC engages other second messenger pathways. For example, activation of mGluR1 in Purkinje cells drives the postsynaptic production of endocannabinoids, which function as diffusible retrograde messengers to transiently depress transmitter release[28].□

Methods

Cell biology assays

Detergent (1% Triton) lysates of rat cerebellum and cell lines were generated and analysed as described[22]. TRPC constructs, cell culture and transfection methods are as described[22]. A total of 100 μl lysates precipitated with 2 μg of anti-TRPC1 antibodies (Alomone). For the negative control, 2 μg of anti-TRPC1 antibodies were preabsorbed with equal amounts of TRPC1 peptide antigen (amino acids 523–537 TRPC1) for 6 h at 4 °C. TRPC1 point mutant F561A was generated by QuikChange site-directed mutagenesis (Stratagene).

Immuno-electron microscopy and immunogold quantification

Immuno-electron microscopy was performed by post-fixation immunogold labelling[29] using a TRPC1 antibody (Alomone) at a dilution of 1:100. A monoclonal mGluR1α antibody[29] was used for double labelling. Brightness and contrast of micrographs were modified using Adobe Photoshop. Results of immunogold labelling are shown in Fig. 1d. Pretreatment of the TRPC1 antibody (left panel of bottom row) with the antigen peptide removed 95% of the gold labelling. Counts of gold particles were 2.67 gold particles per synapse for the area of the postsynaptic density (PSD) and 2.80 for the remaining extrasynaptic area of the spine (63 spine synapses from two animals). As the PSD represents about one-third of the area of spine profiles, these counts indicate enrichment of labelling near the PSD. In co-localization studies a total of 96% of spines labelled with mGluR1 also displayed label for TRPC1 on the spine membrane (Fig. 1d, $n = 121$; two animals). The postsynaptic membrane contained 51% and 35% of TRPC1 and mGluR1α membrane labelling, respectively. The perisynaptic region (defined as one-third of the length of the postsynaptic membrane) contained 17% and 38% of TRPC1 and mGluR1α membrane labelling, respectively.

Electrophysiology

Parasagittal slices of the cerebellar vermis (200 μm thick) were prepared from P18–20 Sprague–Dawley rats using a vibrating tissue slicer and ice-cold standard artificial cerebrospinal fluid (ACSF) containing 124 mM NaCl, 5 mM KCl, 1.25 mM Na_2HPO_4, 2 mM $MgSO_4$, 2 mM $CaCl_2$, 26 mM $NaHCO_3$ and 10 mM D-glucose, bubbled with 95% O_2 and 5% CO_2. After a recovery period of 30 min at 37 °C, the slices were placed in a submerged chamber that was perfused at a rate of 2 ml min^{-1} with ACSF supplemented with 5 μM GABAzine to block $GABA_A$ receptors. Experiments were performed using the visualized whole-cell patch-clamp technique at room temperature. The recording electrodes (resistance 4–5 MΩ) were filled with a solution containing 135 mM Cs-methanesulphonate, 10 mM CsCl, 10 mM HEPES, 4 mM Na_2ATP, 0.4 mM Na_3GTP and 0.2 mM EGTA (pH 7.25). Calcium-free extracellular solution was prepared by replacing $CaCl_2$ with $MgCl_2$ and adding 0.2 mM EGTA. $LaCl_3$ was added to a HEPES-based external solution to prevent precipitation. All drugs were purchased from Sigma except for CPCCOEt, SKF 96365, GABAzine and CNQX, which were purchased from Tocris Cookson. Currents were filtered at 1 kHz and digitized at 5 kHz. For parallel fibre stimulation, standard patch pipettes were used and were filled with external saline and placed in the middle third of the molecular layer. Synaptic responses were evoked every 30 s using 12–16 μA pulses (100 μs duration). When burst stimulation was used, the interpulse interval was 10 ms. In some experiments membrane currents were evoked by agonist application using a pressure application system (Picospritzer; 10 p.s.i., 50 ms pulse duration).

For organotypic cerebellar cultures, 200-μm thick parasagittal slices from P10–12 rats were placed in 1 μm Millicell inserts (Becton Dickinson) within sterile 6-well plates. Medium (1.5 ml) was placed under each insert (50% Eagle's basal medium, 20% Hank's balanced salt solution, 25% heat-inactivated horse serum, 30 mM glucose, 5 mM glutamine, 5 mM HEPES, 1 μg ml^{-1} insulin, 0.012% ascorbic acid, and 100 U ml^{-1} penicillin-streptomycin; all from GIBCO BRL) to achieve an interface configuration. Plates were incubated in 5% CO_2 in air at 37 °C. Cultured slices were transfected using the Helios Gene Gun (Bio-Rad) 24 h after slice preparation. To prepare 'bullets', 25 mg of 1 μm gold particles (Bio-Rad) were coated with DNA plasmid combinations (45 μg TRPC1 mutant plus 5 μg EGFP, 45 μg TRPC1 wild type plus 5 μg EGFP, and 45 μg pRK5 (empty plasmid) DNA plus 5 μg EGFP DNA). A minimum of 10 μl each of 0.5 M spermidine and $CaCl_2$ was used, or this volume was increased to match the volume of DNA. Coated, rinsed gold particles were resuspended in 0.06 mg ml^{-1} polyvinylpyrrolidone in ethanol and then loaded into tubing. Particles were accelerated into cultured slices with the gene gun pressurized to 180 p.s.i.. Plates were returned to the incubator immediately and used for recording after 24 h.

CHO cells were bathed in a solution that contained NaCl (140 mM), KCl (5 mM), $CaCl_2$ (2 mM), $MgCl_2$ (1 mM), HEPES (10 mM) and glucose (10 mM), adjusted to pH 7.35 with NaOH, which flowed at a rate of 1 ml min^{-1}. The internal saline was identical to that used in Purkinje cell recordings. Patch electrodes were pulled from N51A glass and yielded a resistance of 3–5 MΩ. Membrane currents were recorded in resistive voltage-clamp mode, filtered at 2 kHz and digitized at 5 kHz. For CHO cell experiments in which voltage-clamp recording and calcium imaging were combined, EGTA was omitted from the internal saline and replaced with 0.2 mM bis-fura-2. Imaging of free calcium was performed as previously described[30]. Experiments were conducted at room temperature. Cells in which R_{input} or R_{series} varied by more than 15% were excluded from the analysis.

Received 21 February; accepted 30 October 2003; doi:10.1038/nature02162.
Published online 12 November 2003.

1. Conn, P. J. & Pin, J.-P. Pharmacology and functions of metabotropic glutamate receptors. *Annu Rev. Pharmacol. Toxicol.* **37,** 205–237 (1997).
2. Nusser, Z., Mulvihill, E., Streit, P. & Somogyi, P. Subsynaptic segregation of metabotropic and ionotropic glutamate receptors as revealed by immunogold localization. *Neuroscience* **61,** 421–427 (1994).
3. Batchelor, A. M., Madge, D. J. & Garthwaite, J. Synaptic activation of metabotropic glutamate receptors in the parallel fibre-Purkinje cell pathway in rat cerebellar slices. *Neuroscience* **63,** 911–915 (1994).
4. Tempia, F., Miniaci, M. C., Anchisi, D. & Strata, P. Postsynaptic current mediated by metabotropic glutamate receptors in cerebellar Purkinje cells. *J. Neurophysiol.* **80,** 520–528 (1998).
5. Tempia, F., Alojado, M. E., Strata, P. & Knopfel, T. Characterization of the mGluR1-mediated electrical and calcium signaling in Purkinje cells of mouse cerebellar slices. *J. Neurophysiol.* **86,** 1389–1397 (2001).
6. Bortolotto, Z. A., Fitzjohn, S. M. & Collingridge, G. L. Roles of metabotropic glutamate receptors in LTP and LTD in the hippocampus. *Curr. Opin. Neurobiol.* **9,** 299–304 (1998).
7. Aiba, A. *et al.* Reduced hippocampal long-term potentiation and context-specific deficit in associative learning in mGluR1 mutant mice. *Cell* **79,** 365–375 (1994).
8. Conquet, F. *et al.* Motor deficit and impairment of synaptic plasticity in mice lacking mGluR1. *Nature* **372,** 237–243 (1994).
9. Kano, M. & Kato, M. Quisqualate receptors are specifically involved in cerebellar synaptic plasticity. *Nature* **325,** 276–279 (1987).
10. Linden, D. J., Dickinson, M. H., Smeyne, M. & Connor, J. A. A long-term depression of AMPA currents in cultured cerebellar Purkinje neurons. *Neuron* **7,** 81–89 (1991).
11. Aiba, A. *et al.* Deficient cerebellar long-term depression and impaired motor learning in mGluR1 mutant mice. *Cell* **79,** 377–388 (1994).
12. Chiamulera, C. *et al.* Reinforcing and locomotor stimulant effects of cocaine are absent in mGluR5 null mutant mice. *Nature Neurosci.* **4,** 873–874 (2001).
13. Hirono, M., Konishi, S. & Yoshioka, T. Phospholipase C-independent group I metabotropic glutamate receptor-mediated inward current in mouse Purkinje cells. *Biochem. Biophys. Res. Commun.* **251,** 753–758 (1998).
14. Knopfel, T., Anchisi, D., Alojado, M. E., Tempia, F. & Strata, P. Elevation of intradendritic sodium concentration mediated by synaptic activation of metabotropic glutamate receptors in cerebellar Purkinje cells. *Eur. J. Neurosci.* **12,** 2199–2204 (2000).
15. Canepari, M., Papageorgiou, G., Corrie, J. E. T., Watkins, C. & Ogden, D. The conductance underlying the parallel fibre slow EPSP in rat cerebellar Purkinje neurons studied with photolytic release of L-glutamate. *J. Physiol. (Lond.)* **533,** 765–772 (2001).
16. Takechi, H., Eilers, J. & Konnerth, A. A new class of synaptic response involving calcium release in dendritic spines. *Nature* **396,** 757–760 (1998).
17. Finch, E. A. & Augustine, G. J. Local calcium signalling by inositol-1,4,5-trisphosphate in Purkinje cell dendrites. *Nature* **396,** 753–756 (1998).
18. Miyata, M. *et al.* Deficient long-term synaptic depression in the rostral cerebellum correlated with impaired motor learning in phospholipase C beta4 mutant mice. *Eur. J. Neurosci.* **13,** 1945–1954 (2001).
19. Tabata, T., Aiba, A. & Kano, M. Extracellular calcium controls the dynamic range of neuronal metabotropic glutamate receptor responses. *Mol. Cell. Neurosci.* **20,** 56–68 (2002).
20. Hartmann, J. *et al.* Gαq-dependence of mGluR-mediated synaptic signaling in cerebellar Purkinje cells. *Soc. Neurosci. Abstr.* **339.15** (2002).
21. Xiao, B., Tu, J. C. & Worley, P. F. Homer: a link between neural activity and glutamate receptor function. *Curr. Opin. Neurobiol.* **10,** 370–374 (2000).
22. Yuan, J. P. *et al.* Homer binds TRPC family channels and is required for gating of TRPC1 by IP3 receptors. *Cell* **114,** 777–789 (2003).
23. Montell, C., Birnbaumer, L. & Flockerz, V. The TRP channels, a remarkably functional family. *Cell* **108,** 595–598 (2002).
24. Strubing, C., Kraplvinsky, G., Kraplvinsky, L. & Clapham, D. E. TRPC1 and TRPC5 form a novel cation channel in mammalian brain. *Neuron* **29,** 645–655 (2001).
25. Gee, C. E., Benquet, P. & Gerber, U. Group I metabotropic glutamate receptors activate a calcium-sensitive transient receptor potential-like conductance in rat hippocampus. *J. Physiol. (Lond.)* **546,** 655–664 (2003).
26. Tozzi, A. *et al.* Involvement of transient receptor potential-like channels in responses to mGluR1 activation in midbrain dopamine neurons. *Eur. J. Neurosci.* **18,** 2133–2145 (2003).
27. Hofmann, T., Schaefer, M., Schultz, G. & Gudermann, T. Subunit composition of mammalian transient receptor potential channels in living cells. *Proc. Natl Acad. Sci. USA* **99,** 7461–7466 (2002).
28. Maejima, T., Hashimoto, K., Yoshida, T., Aiba, A. & Kano, M. Presynaptic inhibition caused by a retrograde signal from metabotropic to cannabinoid receptors. *Neuron* **31,** 463–475 (2001).
29. Petralia, R. S. *et al.* Glutamate receptor targeting in the postsynaptic spine involves mechanisms that are independent of myosin Va. *Eur. J. Neurosci.* **13,** 1722–1732 (2001).
30. Narasimhan, K., Pessah, I. N. & Linden, D. J. Inositol-1,4,5-trisphosphate receptor-mediated Ca mobilization is not required for cerebellar long-term depression in reduced preparations. *J. Neurophysiol.* **80,** 2963–2974 (1998).

Supplementary Information accompanies the paper on **www.nature.com/nature**.

Acknowledgements We thank R. Bock for technical assistance, C. Montell and T. Hofmann for advice on TRP channels, and Y.-X. Wang for help with electron microscopy immunohistochemistry. This work was supported by USPHS grants to P.F.W. and D.J.L., and by the Develbiss Fund (D.J.L.).

Competing interests statement The authors declare that they have no competing financial interests.

Correspondence and requests for materials should be addressed to D.J.L. (dlinden@jhmi.edu) or P.F.W. (pworley@jhmi.edu).

Testis determination requires insulin receptor family function in mice

Serge Nef[1]*†, Sunita Verma-Kurvari[1]*, Jussi Merenmies[1]†, Jean-Dominique Vassalli[2], Argiris Efstratiadis[3], Domenico Accili[4] & Luis F. Parada[1]

[1]*Center for Developmental Biology, University of Texas, Southwestern Medical Center, 6000 Harry Hines Boulevard, Dallas, Texas 75390-9133, USA*
[2]*University of Geneva, Department of Morphology, Centre Médical Universitaire, 1 rue Michel Servet, 1211 Geneva 4, Switzerland*
[3]*Department of Genetics and Development, and* [4]*Naomi Berrie Diabetes Center & Department of Medicine, College of Physicians & Surgeons of Columbia University,New York, New York 10032, USA*

* These authors contributed equally to this work
† Present Addresses: University of Geneva, Department of Morphology, Centre Médical Universitaire, 1 rue Michel Servet, 1211 Geneva 4, Switzerland (S.N.); University of Helsinki, Hospital for Children and Adolescents, Pediatric Nephrology Unit, Developmental and Reproduction Biology, Bioomedicum Helsinki, Room B526b, PO Box 700 (Haartmanninkatu 8), FIN-00029 HUS, Finland (J.M.)

In mice, gonads are formed shortly before embryonic day 10.5 by the thickening of the mesonephros and consist of somatic cells and migratory primordial germ cells[1]. The male sex-determining process is set in motion by the sex-determining region of the Y chromosome (Sry), which triggers differentiation of the Sertoli cell lineage. In turn, Sertoli cells function as organizing centres and direct differentiation of the testis. In the absence of *Sry* expression, neither XX nor XY gonads develop testes[2], and alterations in *Sry* expression are often associated with abnormal sexual differentiation[3–8]. The molecular signalling mechanisms by which Sry specifies the male pathway and models the undifferentiated gonad are unknown. Here we show that the insulin receptor tyrosine kinase family, comprising Ir, Igf1r and Irr, is required for the appearance of male gonads and thus for male sexual differentiation. XY mice that are mutant for all three receptors develop ovaries and show a completely female phenotype. Reduced expression of both *Sry* and the early testis-specific marker *Sox9* indicates that the insulin signalling pathway is required for male sex determination.

The insulin family signalling pathway is essential for normal growth and development in mice and comprises Ir, Igf1r and Irr. In mice, both Ir and Igf1r are necessary for pre- and postnatal growth and for development. *Ir* mutant pups die from ketoacidosis within 4 d of birth[9,10]. *Igf1r* mutant mice die at birth because of respiratory failure and show several abnormalities including reduced size[11]. Mice lacking both *Ir* and *Igf1r* are even more severely affected[12]. By contrast, mice mutant for *Irr* are viable and do not show overt deficiencies, and so far no physiological function has been attributed to this receptor[13]. The identification of Ir–Igf1r and Ir–Irr hybrid receptors suggests that there is additional complexity in the signalling potential of this family (see refs 14, 15, and references therein). By using mice with mutations at each of the known genes of insulin receptor tyrosine kinase family members (*Ir*, *Igf1r* and *Irr*), here we provide *in vivo* evidence that insulin receptor family function is a precondition for the induction of testicular differentiation by Sry-dependent processes.

By scanning electron microscopy[16], we analysed the developing genito-urinary system at embryonic day 18.5 (E18.5) in male and female mice that were singly mutant for *Ir*, *Irr* and *Igf1r*, as well as doubly or triply mutant for each of the possible combinations. Normal development of the genito-urinary system, including normal intra-abdominal testicular descent, was observed in wild-type and mutant male mice lacking *Ir*, *Irr*, *Igf1r*, *Ir* and *Irr*, or *Igf1r* and *Irr* (Supplementary Fig. 1 and data not shown). By contrast, no *Ir Irr Igf1r* triple mutant embryos ($n = 15$) showed a male phenotype, as determined by the presence of descended testes (Supplementary Fig.1), whereas some *Ir Igf1r* double and compound mutant embryos had partially descended gonads (see below). To rule out selective death of triple mutant XY embryos, the presence of Y chromosome was validated by karyotypic ($n = 1$) and molecular ($n = 4$) analysis for the presence of Y-chromosome-specific markers (*Sry*, *Zfy* and *Ubely*; Supplementary Fig. 2).

We carried out histological analysis at E17.5, when the male and female genito-urinary systems are well developed. Similar to wild-type embryos, single and various double mutant embryos showed sexually dimorphic histology (except for the *Ir Igf1r* double mutant, see below). In all cases, XX embryos had gonads adjacent to the lower pole of the kidney (Supplementary Fig. 3), whereas the XY gonads were significantly larger and lay at a more caudal position adjacent to the bladder. Figure 1 shows, with exception of the triple mutant, the larger size of male (XY) gonads and the presence of seminiferous tubules. By contrast, the XY triple mutant gonad, in addition to being situated adjacent to the kidney, was histologically indistinguishable from XX gonads with no evidence of seminiferous tubules (Fig. 1h, left and right).

To determine whether morphological sex reversal in XY triple mutants was reflected accurately at the molecular level, markers specific for male (*P450scc*, *Insl3*, *Dhh*, *Mis* and *Sox9*) and female (*Wnt4* and *Figα*) gonads were examined by *in situ* hybridization[17–19]. None of the testis-specific genes was expressed in triple mutant XY gonads (Fig. 2). By contrast, the expression of female-specific genes in triple mutant XY gonads was indistinguishable from that in normal or mutant XX gonads. Thus, in addition to phenotypic conversion, the XY gonads of triple mutant embryos express the molecular profiles of normally developing female gonads.

In development, the testicular hormones Mis and testosterone induce regression of the presumptive female tracts (Müllerian ducts) and stabilization of the Wolffian ducts, respectively. To evaluate the consequences of testicular differentiation impairment in XY triple mutant embryos, we analysed the development of the two reproductive tracts. The genital ducts of *Ir Irr* and *Igf1r Irr* double mutants and *Irr* single mutants were sexually dimorphic and indistinguishable from those of wild-type embryos (Supplementary Fig. 4). By contrast, the ducts of all *Ir Igf1r Irr* triple mutant XY embryos resembled the XX structure and showed molecular profiles characteristic of females, including expression of *Wnt4*, *Mis receptor type II* (*MisRII*) and *Wnt7a*[20] (Supplementary Fig. 4). These data are consistent with the absence of Sertoli and Leydig cell differentiation.

To examine when insulin receptor family signalling loss affected testicular differentiation, we assessed the presence of early markers including Sox9 and Mis. Expression of Sox9 is male-specific at E12.5 and is both necessary and sufficient for male sexual determination[21]. At E12.5, XY *Ir Igf1r Irr* triple mutant mice (XY, $n = 5$; XX, $n = 3$) showed substantially less *Sox9* expression than did XY control mice (Fig. 3a, b). Although small amounts of *Sox9* transcripts were detectable in triple mutant XY genital ridges at E12.5, these were apparently insufficient to activate expression of *Mis* (Fig. 3e). In addition, E12.5 triple mutant XY gonads did not express *P450scc*, but upregulation of female-specific *Wnt4* expression was observed ($n = 3$; data not shown). At E13.5 (XY, $n = 3$) no male-specific markers were detected, but at E14.5 (XY, $n = 1$) expression of